Analysis of XL-Array with Near-Field EM Channels

(Invited Paper)

Kangda Zhi[1], Cunhua Pan[2], Tuo Wu[1], Hong Ren[2], and Kok Keong Chai[1]
[1]EECS, Queen Mary University of London, {k.zhi, tuo.wu, michael.chai}@qmul.ac.uk
[2]National Mobile Communications Research Laboratory, Southeast University, {cpan, hren}@seu.edu.cn

***Abstract*—Extremely large-scale array (XL-array) is capable of supporting extremely high system capacity with large numbers of users. In this work, we analyze the performance of discrete-aperture XL-array using the electromagnetic (EM) channel model with near-field spherical wave-front. We derive the explicit signal-noise-ratio (SNR) expressions and based on which the impact of discrete aperture and polarization mismatch is unveiled. We also review the amplitude-aware Fraunhofer distance based on the EM channel model which provides useful insights for distinguishing the boundary between the near-field and far-field.**

***Index Terms*—Extremely-large-scale array, electromagnetic channel model, near-field.**

I. Introduction

As the evolution of massive MIMO, extremely large-scale array (XL-array) has attracted great interest in academia [1], [2]. By mounting more than several thousands of antennas, XL-array can achieve extremely high spectral efficiency and satisfy the harsh criterion of the next-generation communication systems. However, due to the increased aperture of the XL-array, the spherical electromagnetic (EM) wave can no longer be approximated as planar EM wave and the near-field condition should be considered. There are multiple differences between near-field and far-field communications. The first one is the nonlinear variation of the phase of received signal across the whole array. Under the far-field condition, the phase of array steer vector can be approximated as linear for different elements which bring tractable property for mathematical analysis. However, this nature does not hold in the near-field. Secondly, as the array aperture increases, it is essential to consider the amplitude/pathloss variation between different antennas. This is because the distances between the array center and array edge could have significantly different distances between them and the user, which results in amplitude variations. Thirdly, for user located close to XL-array, the signal will have obviously different incline angles which changes the effective projected aperture. Therefore, in the study of XL-array, it is crucial to utilize the practical spherical wave model and then investigate the new nature brought by the near-field communications.

Considering the near-field behavior, XL-array has been studied recently from different perspectives. Focusing on the nonlinear phases of the array steer vector, some research has investigated the problem of beam training [3] and channel estimation [4]. To further accurately model the near-field spherical wave-front, the variation of the amplitude was considered in [5]–[9]. Specifically, the authors in [5] modeled the near-field channel with amplitude variation and took into consideration of different signal incline angles. Based on the EM channel model, the impact of polarization mismatch was considered in [6], [7], which accurately describes the physical near-field behaviors. These works proved that due to the amplitude variation, even though the array aperture tends to be infinitely large, the received power of the signal is still limited. However, for tractability, the above work [5]–[9] has assumed the array to be spatial continuous, i.e., edge-to-edge deployed antennas with zero antenna spacing or infinitely large numbers of infinitesimal antennas. This structure increases the performance but also brings high fabrication complexity and antenna coupling. Thus, the discrete XL-array with half-wavelength spacing was studied in [10]–[12]. However, these works did not adopt the EM channel model and therefore the impact of polarization mismatch cannot be characterized.

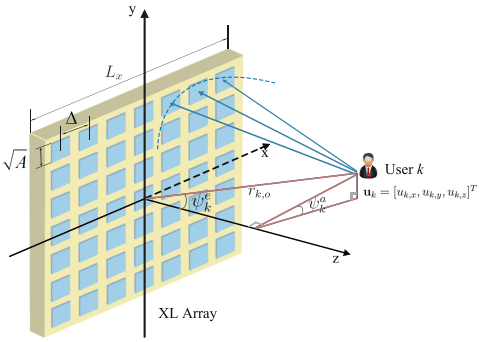

Fig. 1. Illustration of the considered system.

To fill the above research gap, this work investigates the discrete-aperture XL-array with EM channel model. Based on the EM channel model, we derive the explicit SNR expression for discrete-aperture XL-array in the single-user setup. We theoretically unveil the near-field behavior on the SNR performance with the impact of discrete aperture and the polarization mismatch. We also re-examine the amplitude-aware Fraunhofer distance in the presence of polarization mismatch.

II. System Model

As illustrated in Fig. 1, we consider the uplink transmission from a single-antenna user to an XL-array. The Cartesian coordinate system is established in which the origin is the center of the array. Without loss of generality, the user is referred as to user k and its coordinate is denoted by $\mathbf{u}_k = [u_{k,x}, u_{k,y}, u_{k,z}]^T$.

The length of the antennas and the antenna spacing are denoted by $\sqrt{A}$ and Δ, respectively, with $\Delta \geq \sqrt{A}$. The XL-array has $M = M_x M_y$ antennas and the area of each antenna

This work was supported by China Scholarship Council (CSC) and the Fundamental Research Funds for the Central Universities, 2242022k60001.

is A. For brevity, define $\eta = \frac{A}{\Delta^2} \leq 1$ as the array occupation ratio. Considering the (m_x, m_y)-th antenna, the coordinate of its center can be expressed as $\mathbf{p}_{m_x,m_y} = [m_x\Delta, m_y\Delta, 0]^T$, where $m_c \in \left\{-\frac{M_c-1}{2}, \ldots, -1, 0, 1, \ldots, \frac{M_c-1}{2}\right\}, c \in \{x, y\}$. Besides, the area of the (m_x, m_y)-th antenna is denoted as $S_{m_x,m_y} = \left[m_x\Delta - \frac{\sqrt{A}}{2}, m_x\Delta + \frac{\sqrt{A}}{2}\right] \times \left[m_y\Delta - \frac{\sqrt{A}}{2}, m_y\Delta + \frac{\sqrt{A}}{2}\right]$. Then, the distance between the user k and the center of the (m_x, m_y)-th array element is given by $\left\|\mathbf{r}_{k,m_x,m_y}\right\|$, where $\mathbf{r}_{k,m_x,m_y} = \mathbf{p}_{m_x,m_x} - \mathbf{u}_k$. The channel from the user k to the (m_x, m_y)-th antenna of the XL-array is denoted by $h_{k,m_x,m_y} = \sqrt{\xi_{k,m_x,m_y}} e^{-j\frac{2\pi}{\lambda} r_{k,m_x,m_y}}$, where ξ_{k,m_x,m_y} is the channel power/pathloss. Then, combining h_{k,m_x,m_y} for all m_x, m_y into a vector, the channel $\mathbf{h}_k \in \mathbb{C}^{M\times 1}$ from user k to the whole array can be formed.

We apply the Dyadic Green's function-based channel modeling for pathloss ξ_{k,m_x,m_y} [6], [7], [13]. This channel model is more practical and takes the impact of EM polarization into consideration. Specifically, consider a point $\mathbf{p} = [p_x, p_y, 0]^T$ which located in the area of (m_x, m_y)-th antenna, i.e., $\mathbf{p} \in S_{m_x,m_y}$. Based on the Maxwell equations, the electric field of user k satisfies the following inhomogeneous Helmholtz wave equation [6]

$$\left(-\nabla_{\mathbf{u}_k} \times \nabla_{\mathbf{u}_k} \times + k_0^2\right) \boldsymbol{\mathcal{E}}(\mathbf{u}_k) = jk_0\kappa \boldsymbol{\mathcal{J}}(\mathbf{u}_k), \tag{1}$$

where $k_0 = \frac{2\pi}{\lambda}$ is the wavenumber, κ is the intrinsic impedance, and $\boldsymbol{\mathcal{E}}(\mathbf{u}_k)$ is the electric field excited by a current density $\boldsymbol{\mathcal{J}}(\mathbf{u}_k)$. The inverse map of (1) is given by $\boldsymbol{\mathcal{E}}(\mathbf{p}) = \int \boldsymbol{\mathcal{G}}(\mathbf{p}, \mathbf{u}_k)\boldsymbol{\mathcal{J}}(\mathbf{u}_k)d\mathbf{u}_k$. In EM theory, $\boldsymbol{\mathcal{G}}(\mathbf{p}, \mathbf{u}_k)$ is referred as to the Green function which in the radiated near-field can be approximately expressed as [13]

$$\boldsymbol{\mathcal{G}}(\mathbf{p}, \mathbf{u}_k) \approx \frac{j\kappa e^{j\frac{2\pi}{\lambda}\|\mathbf{r}_k\|}}{2\lambda\|\mathbf{r}_k\|} \left(\mathbf{I}_3 - \hat{\mathbf{r}}_k\hat{\mathbf{r}}_k^H\right), \tag{2}$$

where $\mathbf{r}_k = \mathbf{p} - \mathbf{u}_k = [p_x - u_{k,x}, p_y - u_{k,y}, -u_{k,z}]^T$ and $\hat{\mathbf{r}}_k = \frac{\mathbf{r}_k}{\|\mathbf{r}_k\|}$. For notional simplicity, define $r_k = \|\mathbf{r}_k\|$. The Green function $\boldsymbol{\mathcal{G}}(\mathbf{p}, \mathbf{u}_k)$ characterizes the EM response at the point $\mathbf{p}$ due to the current source at point $\mathbf{u}_k$. In this work, the low-cost uni-polarized antenna is considered and the current is assumed to be exited in the y-axis direction [6], [7]. Therefore, the current of the source can be written as $\boldsymbol{\mathcal{J}}(\mathbf{u}_k) = \boldsymbol{\mathcal{J}}_y(\mathbf{u}_k)\hat{\mathbf{e}}_y$ and the pathloss between user k and the (m_x, m_y)-th antenna S_{m_x,m_x} can be modeled as follows

$$\xi_{k,m_x,m_y} = \int_{S_{m_x,m_x}} \frac{\lambda^2}{\kappa^2\pi} \left\|\boldsymbol{\mathcal{G}}(\mathbf{p}, \mathbf{u}_k)\boldsymbol{\mathcal{J}}(\mathbf{u}_k)\right\|^2 \frac{\mathbf{r}_k^T\hat{\mathbf{e}}_z}{\|\mathbf{r}_k\|} d\mathbf{p} \tag{3}$$

$$= \int_{S_{m_x,m_x}} \frac{1}{4\pi r_k^2} \frac{u_{k,z}}{r_k} \frac{(p_x - u_{k,x})^2 + u_{k,z}^2}{r_k^2} d\mathbf{p} \tag{4}$$

$$\overset{\mathbf{p}\approx\mathbf{p}_{m_x,m_y}}{\approx} \frac{A}{4\pi} \frac{u_{k,z}\left((m_x\Delta - u_{k,x})^2 + u_{k,z}^2\right)}{\left\{(m_x\Delta - u_{k,x})^2 + (m_y\Delta - u_{k,y})^2 + u_{k,z}^2\right\}^{\frac{5}{2}}}, \tag{5}$$

where (3) applies a normalized factor $\frac{\lambda^2}{\kappa^2\pi}$ and a projection factor $\frac{\mathbf{r}_k^T\hat{\mathbf{e}}_z}{\|\mathbf{r}_k\|}$ which project the signal to the normal direction to characterize the performance loss due to the angle of incidence deviation. In (5), since the size of each antenna is much smaller than the distance r, all the point $\mathbf{p}$ on area S_{m_x,m_x} is approximated as the center point $\mathbf{p}_{m_x,m_y}$. In (4), it is shown that the utilized pathloss is comprised of three components, including the free-space pathloss $\frac{1}{4\pi r_k^2}$, the propagation projection $\frac{u_{k,z}}{r_k}$, and the polarization mismatch $\frac{(p_x-u_{k,x})^2+u_{k,z}^2}{r_k^2}$ [7]. Clearly, if $u_{k,x} = u_{k,y} = 0$, then $\frac{u_{k,z}}{r_k} = 1$; if $u_{k,y} = p_y$, then $\frac{(p_x-u_{k,x})^2+u_{k,z}^2}{r_k^2} = 1$ and (5) degrades to the pathloss model in [10, (2)]. Thus, compared with [10], the utilized model is more general and can be used to analyze the impact of polarization mismatch.

III. SNR Analysis

The signal received at the XL-array is expressed as $\mathbf{y}_k = \sqrt{p}\mathbf{h}_k x_k + \mathbf{n}$, where p is the transmit power and $\mathbf{n} \sim \mathcal{CN}(\mathbf{0}, \sigma^2\mathbf{I}_M)$. Based on the MRC detector, the SNR is calculated as

$$\mathrm{SNR}_k = \frac{p}{\sigma^2}\|\mathbf{h}_k\|^2 = \frac{p}{\sigma^2}\sum_{m_x}\sum_{m_y}\xi_{k,m_x,m_y}, \tag{6}$$

where ξ_{k,m_x,m_y} is given in (5). In the following, we will present the explicit expression of (6) instead of the form with double-sum. The proof is presented in [14] and omitted here due to the limited space.

Theorem 1 *If $u_{k,z} = 0$, we have $\mathrm{SNR}_k = 0$. Otherwise, the SNR is given by*

$$\begin{aligned}\mathrm{SNR}_k = \frac{p\eta}{6\pi\sigma^2}\Bigg\{&F_k\left(\tfrac{M_y\Delta}{2} - u_{k,y}, \tfrac{M_x\Delta}{2} - u_{k,x}\right)\\ &+F_k\left(\tfrac{M_y\Delta}{2} - u_{k,y}, \tfrac{M_x\Delta}{2} + u_{k,x}\right)\\ &+F_k\left(\tfrac{M_y\Delta}{2} + u_{k,y}, \tfrac{M_x\Delta}{2} - u_{k,x}\right)\\ &+F_k\left(\tfrac{M_y\Delta}{2} + u_{k,y}, \tfrac{M_x\Delta}{2} + u_{k,x}\right)\Bigg\},\end{aligned} \tag{7}$$

where $F_k(a,b) = \arctan\left(\frac{a}{u_{k,z}}\frac{b}{\sqrt{b^2+a^2+u_{k,z}^2}}\right) + \frac{u_{k,z}}{2}\frac{a}{a^2+u_{k,z}^2}\frac{b}{\sqrt{b^2+a^2+u_{k,z}^2}}$.

For large M, we have $M_c\Delta \approx L_c$, $c \in \{x, y\}$, and therefore the SNR in (7) can be further approximated as a function of surface area L_x, L_y, user location $\mathbf{u}_k$, and array occupation ratio $\eta = \frac{A}{\Delta^2} \leq 1$. It embodies the impact of discrete array compared with continuous array from the factor η. Clearly, the SNR is an increasing function with η since $\eta L_x L_y$ represents the effective array aperture. Next, we want to analyze the impact of polarization mismatch on the SNR when using discrete array. Substituting $\frac{(p_x-u_{k,x})^2+u_{k,z}^2}{r_k^2} = 1$ into (4), we can derive the SNR without polarization mismatch, which has the same form as (7) but with inner function $F_k^{w/o}(a,b) = \frac{3}{2}\arctan(\frac{ab}{u_{k,z}\sqrt{a^2+b^2+u_{k,z}^2}})$.

It can be seen that the function $F_k(a,b)$ is more complex than $F_k^{w/o}(a,b)$, which makes theoretical analysis more challenging. Recall that the current with y-axis polarization direction is considered. As a result, the polarization mismatch increases with the difference in y-coordinates between the user and the antenna. Thus, when $L_y \to \infty$ (in severe near-field), we can observe that $\mathrm{SNR}_k^{w/o} \to \frac{3}{2}\mathrm{SNR}_k$, which clearly

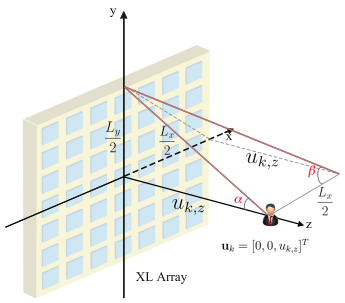

Fig. 2. Geometric understanding for the SNR.

demonstrates the performance loss caused by polarization mismatch. Besides, for large $u_{k,z}$ (i.e., in far-field) and $u_{k,z} \gg a$, we have $\arctan(\frac{a}{u_{k,z}} \frac{b}{\sqrt{b^2+a^2+u_{k,z}^2}}) \approx \frac{ab}{u_{k,z}\sqrt{b^2+a^2+u_{k,z}^2}}$ and $\frac{u_{k,z}}{2} \frac{a}{a^2+u_{k,z}^2} \frac{b}{\sqrt{b^2+a^2+u_{k,z}^2}} \approx \frac{ab}{2u_{k,z}\sqrt{b^2+a^2+u_{k,z}^2}}$, which results in $F_k(a,b) \approx F_k^{w/o}(a,b)$ and accordingly $\mathrm{SNR}_k \approx \mathrm{SNR}_k^{w/o} \approx \frac{p}{\sigma^2} \frac{1}{4\pi r_{k,o}^2} MA\cos\psi_k^e$ [10]. This shows that the polarization mismatch will play more roles in the near-field than far-field, and its impact is more related to parameter a, i.e., L_y and $u_{k,y}$.

In massive MIMO systems with far-field condition and free-space pathloss [15]–[17], the SNR in the single-user scenario is $\mathrm{SNR}_k^{\mathrm{far}} = \frac{p}{\sigma^2} \frac{\lambda^2}{(4\pi)^2 r_{k,o}^2} M$, which increases linearly with M to infinity. However, we know that the received power cannot exceed the transmitted power based on energy conservation. In fact, when $M \to \infty$, the near-field channel model should be applied and the linear scale in $\mathrm{SNR}_k^{\mathrm{far}}$ no longer holds. Based on the EM near-field channel, when $M \to \infty$, the SNR converges to

$$\mathrm{SNR}_k \to \frac{p}{\sigma^2} \frac{4\eta}{6\pi} F_k\left(\frac{L_y}{2}, \frac{L_x}{2}\right) \to \frac{p}{\sigma^2} \frac{\eta}{3}. \tag{8}$$

If the polarization mismatch is neglected, the asymptotic SNR is

$$\mathrm{SNR}_k^{w/o} \to \frac{p}{\sigma^2} \frac{\eta}{\pi} F_k^{w/o}\left(\frac{L_y}{2}, \frac{L_x}{2}\right) \to \frac{p}{\sigma^2} \frac{\eta}{2}. \tag{9}$$

If the array is assumed to be continuous i.e., $\sqrt{A} = \Delta$, we have

$$\mathrm{SNR}_k^{\mathrm{cont}} \to \frac{p}{\sigma^2} \frac{1}{3}. \tag{10}$$

The results in (8) - (10) provide the practical performance limit when the XL-array has an infinitely-large surface area. It can be seen that our result (8) is smaller compared with the other two cases. In (9), at most half of the power can be received by an infinitely large array surface, since it can only occupy half of the space. With polarization mismatch, the limit reduces to $1/3$. This is because as L_y increases, the attenuation from the source to the edge of the array caused by polarization mismatch becomes severer. Intuitively, the array occupation ratio η also plays a key role in the limit since it represents the effective surface area.

The reason why the SNR is limited with $M \to \infty$ can also be explained from the perspective of geometric angles. For ease of understanding, consider a user located perpendicular to the center of the array, i.e., $u_{k,x} = u_{k,y} = 0$. In this case, as illustrated in Fig. 2, we define two angles α and β so that $\tan\alpha = \frac{L_y/2}{u_{k,z}}$ and $\cos\beta = \frac{L_x/2}{\sqrt{\left(\frac{L_x}{2}\right)^2+\left(\frac{L_y}{2}\right)^2+u_{k,z}^2}}$. Then, the SNR can be re-written as

$$\mathrm{SNR}_k^{\mathrm{p}} = \frac{p}{\sigma^2} \frac{2\eta}{3\pi} \left\{ \arctan(\tan\alpha\cos\beta) + \frac{1}{2}\sin\alpha\cos\alpha\cos\beta \right\}. \tag{11}$$

The SNR in (11) is a function of angles α and β. As the aperture of the array increases infinitely large, however, the angles of view from the user to the array, i.e., α and β, are still limited. Specifically, if $L_x \to \infty$, there is $\beta \to 0$. When $L_y \to \infty$, there is $\alpha, \beta \to \frac{\pi}{2}$. If both L_x and L_y tend to infinity, there are $\alpha \to \frac{\pi}{2}$ and $\beta \to \frac{\pi}{4}$. As a result, the SNR is limited by the angles and cannot increase infinity.

For better understanding the impact of polarization mismatch, we next consider a simplified case where the XL-UPA degrades to the XL-ULA, i.e., $M_x = 1$ or $M_y = 1$.

Theorem 2 *When $M_y = 1$, the SNR for XL-ULA is given by*

$$\begin{aligned} \mathrm{SNR}_k^{\mathrm{ULA}} = \frac{p}{\sigma^2} \frac{\eta\Delta}{4\pi} \Big\{ & F_k^{\mathrm{ULA}}\left(\frac{M_x\Delta}{2} - u_{k,x}\right) \\ & + F_k^{\mathrm{ULA}}\left(\frac{M_x\Delta}{2} + u_{k,x}\right) \Big\}, \end{aligned} \tag{12}$$

where

$$F_k^{\mathrm{ULA}}(a) = \frac{a\left(a^2u_{k,y}^2+3u_{k,z}^2\left(a^2+u_{k,y}^2+u_{k,z}^2\right)\right)u_{k,z}}{3\left(u_{k,y}^2+u_{k,z}^2\right)^2\left(a^2+u_{k,y}^2+u_{k,z}^2\right)^{\frac{3}{2}}}. \tag{13}$$

The result in (12) is consistent with [10] only if $u_{k,y} = 0$. This is because when $M_y = 1$, the y-coordinate of all antennas on XL-ULA is 0. When the y-coordinate of the user is also $u_{k,y} = 0$, the difference in y-coordinate between the user and all antennas on the ULA is zero and therefore no polarization mismatch exists. For $M_x \to \infty$, the asymptotic limit of the SNR is

$$\mathrm{SNR}_k^{\mathrm{ULA}} \overset{M\to\infty}{\to} \frac{p}{\sigma^2} \frac{A}{2\pi\Delta} \frac{u_{k,z}\left(u_{k,y}^2+3u_{k,z}^2\right)}{3\left(u_{k,y}^2+u_{k,z}^2\right)^2}. \tag{14}$$

It can be seen that (14) is unrelated to $u_{k,x}$. This is because as $M_x \to \infty$, the array is infinitely long and therefore the x-coordinate of the user does not matter. Furthermore, the asymptotic SNR for XL-ULA without polarization mismatch is given by

$$\mathrm{SNR}_{k,\mathrm{w/o}}^{\mathrm{ULA}} \overset{M\to\infty}{\to} \frac{p}{\sigma^2} \frac{A}{2\pi\Delta} \frac{u_{k,z}\left(3u_{k,y}^2+3u_{k,z}^2\right)}{3\left(u_{k,y}^2+u_{k,z}^2\right)^2} \geq \mathrm{SNR}_k^{\mathrm{ULA}}, \tag{15}$$

and the gap between (14) and (15) is

$$D_{\mathrm{SNR}_k} = \mathrm{SNR}_{k,\mathrm{w/o}}^{\mathrm{ULA}} - \mathrm{SNR}_k^{\mathrm{ULA}} = \frac{p}{\sigma^2} \frac{A}{3\pi\Delta} \frac{u_{k,z}u_{k,y}^2}{\left(u_{k,y}^2+u_{k,z}^2\right)^2}, \tag{16}$$

which first increases and then decreases with respect to $u_{k,y}$. Specifically, we have $D_{\mathrm{SNR}_k} \to 0$ as $u_{k,y} \to 0$ and $D_{\mathrm{SNR}_k} \to 0$ as $u_{k,y} \to \infty$. This is rational. When $u_{k,y} = 0$, the user possesses the same y-coordinate as the whole ULA,

and therefore the polarization mismatch vanishes. As $u_{k,y}$ increases, the difference of the y-coordinate increases leading to larger polarization mismatch. However, for large enough $u_{k,y}$, the user will be located in the far-field and therefore the gap vanishes.

A. The Field Boundaries

In this section, we aim to revisit the boundary between the near-field and the far-field based on the discrete array with polarization mismatch. The classic Fraunhofer distance [18], i.e., $d_f = \frac{2D^2}{\lambda}$, mainly focuses on the variation of the phase between different antennas while the pathloss variation of ξ_{k,m_x,m_y} across different antennas is ignored. In [10], an amplitude-aware Fraunhofer distance is proposed. Inspired by [10], we further take the impact of polarization mismatch into consideration, which is more general and more challenging. Based on the amplitude model of the considered discrete-aperture XL-MIMO array, we quantify the amplitude variation across the whole array as follows

$$\mathrm{v}(\mathbf{u}_k) = \frac{\min_{m_x,m_y} \xi_{k,m_x,m_y}}{\max_{m_x,m_y} \xi_{k,m_x,m_y}}. \tag{17}$$

For $\mathbf{u}_k$ located in the far-field with planar wave-front, we have $\mathrm{v}(\mathbf{u}_k) = 1$. As the user moves closer to the array, the near-field behavior manifests itself, and the variation of the amplitude across the array becomes non-negligible. Therefore, we can define an amplitude variation threshold $\bar{\mathrm{v}}_t \in (0, 1]$, and then determine the near/far-field boundary by finding the set of locations $\tilde{\mathbf{u}}_k$, where $\mathrm{v}(\tilde{\mathbf{u}}_k) = \bar{\mathrm{v}}_t$. Clearly, the field boundary will be a surface comprised of 3D user positions. Based on (5), we can find that the amplitude ξ_{k,m_x,m_y} between user k and the (m_x, m_y)-th antenna element decreases with their y-coordinate difference $|m_y\Delta - u_{k,y}|$ but it is not monotonic of their x-coordinate difference $|m_x\Delta - u_{k,x}|$. This is because when $|m_y\Delta - u_{k,y}|$ increases, both the distance and the polarization mismatch increase. By contrast, when $|m_x\Delta - u_{k,x}|$ increases, the distance increases but the relative polarization mismatch decreases.

In the following, we aim to obtain the explicit values of m_x and m_y which respectively maximize and minimize ξ_{k,m_x,m_y} given $\mathbf{u}_k$. By defining $s = (m_x\Delta - u_{k,x})^2 + u_{k,z}^2$ and $v = (m_y\Delta - u_{k,y})^2$, we are able to rewritten ξ_{k,m_x,m_y} as $f_\xi(s) = \frac{s}{(s+v)^{\frac{5}{2}}}$ with $f'_\xi(s) = (s+v)^{\frac{-7}{2}}(v - \frac{3}{2}s)$. For brevity, define $f_{\text{int}}(a) = \lfloor a + \frac{1}{2} \rfloor$ rounding a to the nearest integer. Define $f_{\pm x}(a) = \frac{u_{k,x}}{|u_{k,x}|}a$. Define $f_{|\min|}(a,b)$; if $|a| \le |b|$, $f_{|\min|}(a,b) = a$; if $|a| > |b|$, $f_{|\min|}(a,b) = b$. Then, based on the range of m_x and m_y, we can derive the domain of $s \in [s_{\min}, ..., s_{\max}]$ where $s_{\max} = \left(f_{\pm x}\left(\frac{M_x-1}{2}\right)\Delta + u_{k,x}\right)^2 + u_{k,z}^2$ and

$$s_{\min} = \Big(\Big\{ f_{|\min|}\left(f_{\text{int}}\left(\tfrac{u_{k,x}}{\Delta}\right), f_{\pm x}\left(\tfrac{M_x-1}{2}\right)\right)\Big\}\Delta - u_{k,x}\Big)^2 + u_{k,z}^2. \tag{18}$$

By analyzing the properties of $f_\xi(s)$, we can obtain the following solutions: to maximize $f_\xi(s)$, there are $\overline{m}_y = f_{|\min|}\left\{f_{\text{int}}\left(\frac{u_{k,y}}{\Delta}\right), f_{\pm y}\left(\frac{M_y-1}{2}\right)\right\}$, $v^* = (\overline{m}_y\Delta - u_{k,y})^2$, and

$$\overline{m}_x = \begin{cases} f_{\text{int}}\left(f_{|\min|}\left\{\frac{\sqrt{\frac{2}{3}v^* - u_{k,z}^2} + u_{k,x}}{\Delta}, \frac{-\sqrt{\frac{2}{3}v^* - u_{k,z}^2} + u_{k,x}}{\Delta}\right\}\right) \\ \qquad\qquad , \text{ if } s_{\min} \le \frac{2}{3}v^* \le s_{\max} \\ f_{|\min|}\left\{f_{\text{int}}\left(\frac{u_{k,x}}{\Delta}\right), f_{\pm x}\left(\frac{M_x}{2}\right)\right\}, \text{ if } \frac{2}{3}v^* < s_{\min} \\ -f_{\pm x}\left(\frac{M_x-1}{2}\right), \text{ if } \frac{2}{3}v^* > s_{\max} \end{cases} \tag{19}$$

To minimize $f_\xi(s)$, there are $\underline{m}_y = -f_{\pm y}\left(\frac{M_y}{2}\right)$, $v^* = \left(\underline{m}_y\Delta - u_{k,y}\right)^2$, and

$$\underline{m}_x = \begin{cases} f_{|\min|}\left\{f_{\text{int}}\left(\frac{u_{k,x}}{\Delta}\right), f_{\pm x}\left(\frac{M_x}{2}\right)\right\} \\ \qquad , \text{ if } s_{\min} \le \frac{2}{3}v^* \le s_{\max}, f_\xi(s_{\min}) \le f_\xi(s_{\max}); \\ -f_{\pm x}\left(\frac{M_x-1}{2}\right) \\ \qquad , \text{ if } s_{\min} \le \frac{2}{3}v^* \le s_{\max}, f_\xi(s_{\min}) > f_\xi(s_{\max}); \\ f_{|\min|}\left\{f_{\text{int}}\left(\frac{u_{k,x}}{\Delta}\right), f_{\pm x}\left(\frac{M_x}{2}\right)\right\}, \text{ if } \frac{2}{3}v^* > s_{\max}; \\ -f_{\pm x}\left(\frac{M_x-1}{2}\right), \text{ if } \frac{2}{3}v^* < s_{\min}. \end{cases} \tag{20}$$

Based on (19) and (20), we can calculate $\mathrm{v}(\mathbf{u}_k)$ given $\mathbf{u}_k$. Then, to find the $\tilde{\mathbf{u}}_k = [\tilde{u}_{k,x}, \tilde{u}_{k,y}, \tilde{u}_{k,z}]$ on the field boundary, we can fix $\tilde{u}_{k,x}$ and $\tilde{u}_{k,y}$ and then use the one-dimensional search to find $\tilde{u}_{k,z}$ which leads to $\mathrm{v}(\tilde{\mathbf{u}}_k) = \bar{\mathrm{v}}_t$.

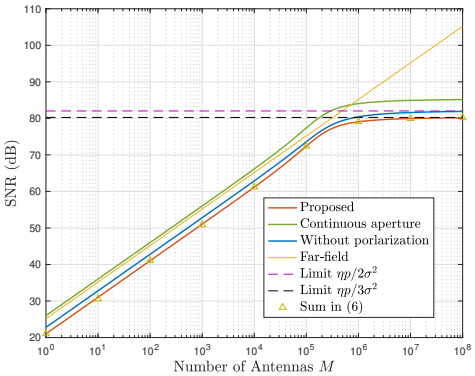

Fig. 3. SNR versus M for XL-UPA, $\mathbf{u}_k = [10, 10, 10]$, $M_x = M_y = \sqrt{M}$.

IV. Simulations

In this section, we provide numerical results for validating our theoretical analysis and draw insights for XL-array-based communication systems. As [10]–[12], we set $\Delta = \frac{\lambda}{2} = 0.0628$ m, $\frac{p}{\sigma^2} = 90$ dB, and $A = \frac{\lambda^2}{4\pi}$.

Fig. 3 illustrates the SNR performance as the aperture of XL-UPA tends to be infinitely large. It can be seen that different from the far-field-based results which increase linearly, the near-field-based SNR first increases but then saturates to a limit as $M \to \infty$. It can be observed that the proposed result, which takes into consideration of discrete aperture and polarization mismatch, characterizes the actual performance with additional loss. Besides, it can be seen that the sum results in (6) are well approximated by the derived explicit results.

In Fig. 4, the asymptotic SNR of XL-ULA is studied. A similar tendency can be found as in Fig. 3. However, the

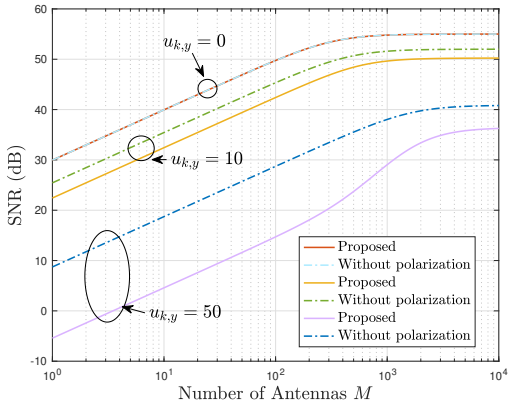

Fig. 4. SNR versus M for XL-ULA, $\mathbf{u}_k = [0, u_{k,y}, 10]$, $M_y = 1$

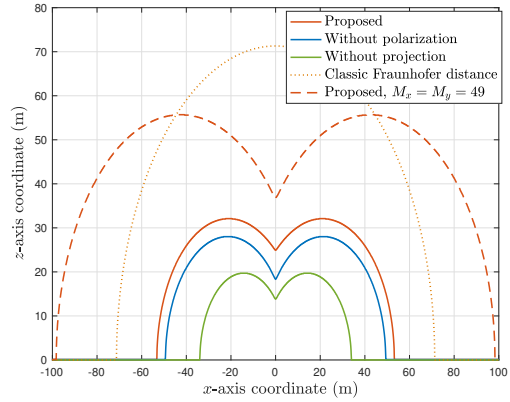

Fig. 5. Field boundaries, $u_{k,y} = 0$, $M_x = M_y = 25$.

number of antennas needed for the SNR to slow down its growth rate is much smaller than that in Fig. 3. With ULA, the SNR turns to saturation with almost 10^3 antennas while the needed number of antennas for UPA is 10^6. This is because given M, the ULA has a much larger dimension than UPA and therefore the variations of the amplitude, the signal incline angles, and the polarization mismatch across the whole array are more obvious on the ULA. Recalling the geometric understanding from Fig. 2, as M increases, the enlarging of the view of angles is easier to saturate in ULA than angles in UPA. Besides, it can be observed that the SNR gap between the proposed model and the model without polarization mismatch enlarges as the y-coordinate of the user increases. This phenomenon agrees with our analytical result (16) since the polarization mismatch is proportional to the difference of y-coordinate between the user and the received antennas. As a result, as $u_{k,y}$ increases, the performance loss caused by polarization mismatch increases.

In Fig. 5, the amplitude-aware Fraunhofer distance is re-examined after taking into consideration the impact of polarization mismatch. The results are shown with $u_{k,y} = 0$. We also present the results when neglecting the polarization mismatch and neglecting both the polarization mismatch and the angle projection. It can be seen that different from the classic phase-aware Fraunhofer distance which is a semicircle, the three amplitude-aware Fraunhofer distances shrink when the user is located face to the center of the array. This is because the variation of amplitude from the center to the edge of the array is milder than that from one edge to the other edge. With milder amplitude variation, the near-field area is smaller. Meanwhile, it can be seen that the considered case has a larger Fraunhofer distance since the polarization mismatch further aggravates the amplitude variation across the array. Besides, It can be seen that the Fraunhofer distance increases with M due to the larger array dimension.

V. Conclusion

In this work, we investigated the performance of XL-array based on the EM channel model with near-field behavior. We derived the explicit expression of SNR in the single-user setup, which provides useful insights for understanding the impact of discrete aperture and polarization mismatch. We also studied the Fraunhofer distance under the proposed EM channel.

References

[1] C. Huang, S. Hu, G. C. Alexandropoulos, A. Zappone, C. Yuen, R. Zhang, M. D. Renzo, and M. Debbah, "Holographic MIMO surfaces for 6G wireless networks: Opportunities, challenges, and trends," *IEEE Wireless Commun.*, vol. 27, no. 5, pp. 118–125, 2020.

[2] Z. Wang, J. Zhang, H. Du, W. E. Sha, B. Ai, D. Niyato, and M. Debbah, "Extremely large-scale MIMO: Fundamentals, challenges, solutions, and future directions," *arXiv preprint arXiv:2209.12131*, 2022.

[3] M. Cui *et al.*, "Near-field rainbow: Wideband beam training for XL-MIMO," *IEEE Trans. Wireless Commun.*, early access, 2022.

[4] M. Cui and L. Dai, "Channel estimation for extremely large-scale MIMO: Far-field or near-field?" *IEEE Trans. Commun.*, vol. 70, no. 4, pp. 2663–2677, Jan. 2022.

[5] S. Hu, F. Rusek, and O. Edfors, "Beyond massive MIMO: The potential of data transmission with large intelligent surfaces," *IEEE Trans. Signal Process.*, vol. 66, no. 10, pp. 2746–2758, May 2018.

[6] D. Dardari, "Communicating with large intelligent surfaces: Fundamental limits and models," *IEEE J. Sel. Areas Commun.*, vol. 38, no. 11, pp. 2526–2537, Nov. 2020.

[7] E. Björnson and L. Sanguinetti, "Power scaling laws and near-field behaviors of massive MIMO and intelligent reflecting surfaces," *IEEE Open J. Commun. Soc.*, vol. 1, pp. 1306–1324, Sep. 2020.

[8] A. de Jesus Torres, L. Sanguinetti, and E. Björnson, "Near-and far-field communications with large intelligent surfaces," in *2020 54th Asilomar Conference on Signals, Systems, and Computers*. IEEE, 2020, pp. 564–568.

[9] L. Wei, C. Huang, G. C. Alexandropoulos, Z. Yang, J. Yang, W. E. Sha, M. Debbah, and C. Yuen, "Channel modeling and multi-user precoding for Tri-polarized holographic MIMO communications," *arXiv preprint arXiv:2302.05337*, 2023.

[10] H. Lu and Y. Zeng, "Communicating with extremely large-scale array/surface: Unified modelling and performance analysis," *IEEE Trans. Wireless Commun.*, Jun. 2021.

[11] ——, "Near-field modeling and performance analysis for multi-user extremely large-scale MIMO communication," *IEEE Commun. Lett.*, vol. 26, no. 2, pp. 277–281, Feb. 2022.

[12] X. Li, H. Lu, Y. Zeng *et al.*, "Near-field modeling and performance analysis of modular extremely large-scale array communications," *IEEE Commun. Lett.*, vol. 26, no. 7, pp. 1529–1533, Jul. 2022.

[13] A. Poon, R. Brodersen, and D. Tse, "Degrees of freedom in multiple-antenna channels: a signal space approach," *IEEE Trans. Inf. Theory*, vol. 51, no. 2, pp. 523–536, Feb. 2005.

[14] K. Zhi *et al.*, "Performance analysis and low-complexity design for XL-MIMO with near-field spatial non-stationarities," *arXiv preprint arXiv:2304.00172*, 2023.

[15] E. Björnson, J. Hoydis, and L. Sanguinetti, "Massive MIMO networks: Spectral, energy, and hardware efficiency," *Found. Trends Signal Process.*, vol. 11, no. 3-4, pp. 154–655, Nov. 2017.

[16] K. Zhi *et al.*, "Two-timescale design for reconfigurable intelligent surface-aided massive MIMO systems with imperfect CSI," *IEEE Trans. Inf. Theory*, early access, 2022.

[17] K. Zhi, C. Pan *et al.*, "Power scaling law analysis and phase shift optimization of RIS-aided massive MIMO systems with statistical CSI," *IEEE Trans. Commun.*, vol. 70, no. 5, pp. 3558–3574, May 2022.

[18] K. T. Selvan and R. Janaswamy, "Fraunhofer and fresnel distances: Unified derivation for aperture antennas." *IEEE Antennas Propag. Mag.,*, vol. 59, no. 4, pp. 12–15, Aug. 2017.